ELSEVIER

Contents lists available at ScienceDirect

## Journal of Archaeological Science

journal homepage: www.elsevier.com/locate/jas





# Classification of Bovidae fossils from Gladysvale, South Africa using elastic shape analysis

Juliet K. Brophy <sup>a,b,\*</sup>, Gregory J. Matthews <sup>c,d</sup>, Nicole Schnitzler <sup>e</sup>, Karthik Bharath <sup>f</sup>, Sebastian Kurtek <sup>e</sup>, Ofer Harel <sup>g</sup>

- <sup>a</sup> Department of Geography and Anthropology, Louisiana State University, USA
- b Centre for the Exploration of the Deep Human Journey, University of the Witwatersrand, Johannesburg, South Africa
- Department of Mathematics and Statistics, Loyola University Chicago, USA
- <sup>d</sup> Center for Data Science and Consulting, Loyola University Chicago, USA
- e Department of Statistics, The Ohio State University, USA
- f School of Mathematical Sciences, University of Nottingham, UK
- g Department of Statistics, University of Connecticut, USA

#### ARTICLE INFO

Keywords:
Shape analysis
Classification
Gladysvale
Bovid teeth
Machine learning
Paleoenvironmental reconstruction

#### ABSTRACT

Teeth from the Family Bovidae that are associated with our early humans ancestors are important for reconstructing paleoenvironments. However, age, degree of attrition, and taphonomic factors often make fossil identification difficult. A recent technique for classifying these teeth uses the size-and-shape of the occlusal surface as a summary of the surface, deriving features from this, and then using these features in machine learning classification algorithms. Bovid teeth have previously been classified using this method with features derived from coefficients of elliptical Fourier analysis (EFA). This study assesses the utility of using other shape representations for feature generation, specifically elastics shape analysis. Features were derived using this frame work for both shape only and size-and-shape (i.e. size is not considered a nuisance parameter), and those features were used as input for machine learning algorithms. We demonstrate that features derived elastic shape analysis generally outperform features derived from EFA in terms of cross validation classification accuracy. Finally, an application of the classification methods studied here was applied to fossils recovered from the deroofed Gladysvale External deposit (GVED), Gauteng Province, South Africa. Previous analyses of GVED identified a group of bovids as medium sized alcelaphines (Lacruz et al., 2002). Specifically, this study reclassified 32 unbroken, medium sized alcelaphines looking at shape and size-and-shape. The reclassifications increased the number of individuals and diversity of bovids recovered from the site. The results were used to generate a more precise paleoenvironmental reconstruction.

## 1. Introduction

Paleoenvironmental reconstruction is an important tool in biological anthropology for studying early human behavior. These reconstructions rely on the animals associated with our fossil human ancestors. Specifically, animals in the Family Bovidae (e.g. antelopes and buffalo) are used because of their environmental tendencies such as their habitats, water dependence or migration patterns (Estes, 2012). Bovids, particularly isolated bovid teeth, are one of the most common fossils recovered from southern African sites. Thus, accurate identification of the tribe and/or species of bovids, based on the collected fossils, is key to effective paleoenvironmental reconstruction. Traditionally, researchers have

used fossil and modern comparative collections when attempting to identify the bovid fossils (de Ruiter et al., 2008; Adams and Conroy, 2005; Vrba, 1976). However, this manual process can be subjective and heavily depend on the human analyst. To remedy this issue, geometric morphometrics in conjunction with machine learning techniques have recently been used to automatically identify isolated bovid teeth by relying on the shape of the outline of the occlusal surface of these teeth, most often through the use of elliptical Fourier analysis (EFA) (Brophy, 2011; Caple et al., 2017).

In particular, Brophy et al. (2014) presents work on classifying fossil bovid teeth, using linear discriminant analysis (LDA) as the classification method, based on covariates derived from the shape of the outline of the

<sup>\*</sup> Corresponding author. Department of Geography and Anthropology, Louisiana State University, USA. *E-mail address*: jbrophy@lsu.edu (J.K. Brophy).

occlusal surface of the tooth via an EFA decomposition. Continuing this line of work, Matthews et al. (2018) again used EFA to decompose the shape into a collection of harmonics coefficients. These coefficients (and their principal components) were used as features in more complex machine learning classifiers such as support vector machines Cortes and Vapnik (1995), random forests Ho (1995); Breiman (2001), nuclear penalized multinomial regression Powers et al. (2018), and neural networks, which were all shown to outperform LDA. These machine learning methods have been shown to work well with features derived from an EFA decomposition of the shape of the occlusal surface of a tooth. However, the EFA decomposition of shape requires the parameterization of the corresponding outlines to be according to arc-length. In practice, due to high shape variability in the outlines of the occlusal surface of bovid teeth, this can result in inefficient shape representation. As such, it may be more suitable to allow flexible parameterizations to ensure more efficient matching of geometric features across bovid tooth

An alternative framework for characterizing shapes without having to rely on EFA is elastic shape analysis (Srivastava and Klassen, 2016; Bharath and Kurtek, 2020). Elastic shape analysis derives shapes from parameterized curves by removing nuisance shape variation, i.e. translation, rotation, parameterization and global scale, via a process called registration. This process essentially aligns two or more shapes optimally to each other with respect to the aforementioned nuisance transformations using a formal distance on the associated shape space. The shape distance can be used to compare shapes numerically and visually (via paths of shortest shape deformation), to compute a sample mean shape, and to summarize variation in a sample of shapes using principal component analysis. In this work, we derive shape features using elastic shape analysis and use them to classify bovid teeth using machine learning approaches. We show that allowing flexible parameterizations of bovid tooth outlines and performing registration to optimally align them with respect to the shape distance results in improved classification results as compared to EFA. Full details of the elastic shape analysis framework can be found in Section 3.1.

Recently, Domínguez-Rodrigo et al. (2023) performed classification of bovid teeth using the actual images of the teeth as input in a deep convolutional neural network (DCNN). Our approach uses features derived exclusively from the shape or size-and-shape of the outline of the occlusal surface of each tooth. While our primary goal in this manuscript and the goal in Domínguez-Rodrigo et al. (2023) are similar, i.e. taxonomic classification of bovid teeth, the methods used to generate features for use in machine learning algorithms to perform this classification are very much different. In particular, the features proposed in our work are based on shape (or shape-and-size) deformation vectors or their principal components. In both cases, the features effectively capture variation within and between classes. Furthermore, the estimated deformation vectors or principal directions of variation used to generate the PC-based features can be easily visualized and potentially interpreted by applied scientists, allowing them to assess which local shape features of the teeth are the driving factors in classification performance. Such visualizations and interpretations are more difficult to generate for image-derived DCNN features. In addition, the results reported in Domínguez-Rodrigo et al. (2023) are not directly comparable to the results presented here as the samples used for training in Domínguez-Rodrigo et al. (2023) are not the same as the training samples used in this work. In the future, we plan to compare these two methods of classification using the same set of images (image-derived shapes).

The presented research pertains to a sample of bovids recovered from Gladysvale, a hominin bearing site located in the Bloubank Valley of the Gauteng Province in the UNESCO Cradle of Humankind World Heritage Area, approximately 13 km northeast of the site of Sterkfontein. The Gladysvale cave system consists of internal deposits (GVID) from a three chambered cave system, and external deposits (GVED) which have been uncovered by erosion and collapse of the cave roof (Lacruz et al., 2002; Pickering et al., 2007). Hominins, fauna and an Acheulean handaxe have

been recovered from the site (Lacruz et al., 2002; Berger et al., 1993; Hall et al., 2006). The deroofed Gladysvale external deposit consists of both calcified and decalcified deposits and dates to approximately 578–780 Ka. (Lacruz et al., 2002). The taphonomy of the bones suggests the fossils were accumulated by both carnivores and porcupines. Previous analyses of the GVED decalcified deposits excavated between 1999 and 2002 identified a group of bovid fossil teeth as medium sized alcelaphines (Lacruz et al., 2002). The four Bovidae Alcelaphini extant species considered in this research are Damaliscus dorcas, Alcelaphus buselaphus, Connochaetes gnou, Connochaetes taurinus; we focused on the taxa most commonly found in the Cradle of Humankind, South Africa in the Plio-Pleistocene. The teeth of these four species overlap in shape and size making them difficult to identify based on the fossil record. Thus, many researchers are forced to group these bovids into broad, ambiguous categories such as medium sized alcelaphines (see e.g. Berger and Lacruz (2003); de Ruiter et al. (2008)). The fact that these teeth are isolated exacerbates the issues with classification. All of these species existed in South Africa during the estimated date of the site (Lacruz et al., 2002).

The purpose of this study is twofold: (1) to compare classification performance of different types of features derived using the elastic shape analysis framework and EFA (baseline), and (2) to use the best performing approach to classify 32, unbroken medium sized alcelaphines to their genera/species using the form (shape and size) of the occlusal surface of the tooth. The presented approach is meant to be a quantifiable, reproducible supplement to fossil tooth identifications. Therefore, the reclassifications will be checked with other features of the teeth such as degree of hypsodonty and central cavity shape, characteristics that do not affect the shape of the tooth. The reclassifications can further be used to generate a more precise paleoenvironmental reconstruction.

#### 2. Data

This study uses the database B.O.V.I.D. (Brophy and Matthews, 2022) which includes extant bovids from 7 tribes and 20 species as reported in Table 1. The training data consists of 3838 outlines of the occlusal surface of bovid teeth (Brophy and Matthews, 2022). There are six tooth types in the database: Lower Molar (LM) 1, 2 and 3, and Upper

**Table 1**Extant bovid list from reference database

Tribe	Species
Alcelaphini	
	Damaliscus dorcas
	Alcelaphus buselaphus
	Connochaetes gnou
	Connochaetes taurinus
Antilopini	
	Antidorcas marsupialis
Neotragini	
	Oreotragus oreotragus
	Ourebia ourebi
	Pelea capreolus
	Raphicerus campestris
Tragelaphini	
	Tragelaphus scriptus
	Tragelaphus strepsicero
	Taurotragus oryx
Bovini	
	Syncerus caffer
Hippotragini	
	Oryx gazella
	Hippotragus equinus
	Hippotragus niger
Reduncini	
	Redunca arundinum
	Redunca fulvorufula
	Kobus leche
	Kobus ellipsiprymnus

Molar (UM) 1, 2 and 3. The teeth in the database are all adult teeth with varying degrees of wear (unworn to old). The database includes different wear stages in an attempt to incorporate normal biological variation (see Brophy and Matthews (2022) for more details). Each tooth type contains at least 600 outlines in the training dataset with the smallest group, LM3, containing 619 records, and the largest group, UM2, containing 657 specimens. The specific sample sizes for each tooth type across the seven tribes considered in this study are provided in Table 2. Note that different tribes have different numbers of species, which is why some tribes have more specimens than others. Classification models will be trained separately for each tooth type (see Section 4).

Fig. 1 illustrates an example of a photograph of a tooth (left) along with the black and white image of the segmented tooth (right). The black and white images of teeth were created using the lasso tool in the open-source GNU Image Manipulation Program (GIMP) (The GIMP Development Team, 2019). The (x, y)-coordinates of the outlines of the segmented teeth were generated using the import jpg function in the Momocs package (Bonhomme et al., 2014) available in R (R Core Team, 2021). Each tooth outline was stored as a  $2 \times N$  matrix, where N represents the number of (x, y)-coordinates along the outline.

#### 3. Methods

We begin by describing the elastic shape analysis framework for shape and size-and-shape analysis, which is used to generate features for bovid tooth shape classification. We then briefly describe the EFA method for feature generation that is used as a baseline. Finally, we describe the classification methods and rules used in this work.

#### 3.1. Elastic shape analysis

Each bovid tooth outline is represented as a parameterized, closed, absolutely continuous planar curve  $\beta : \mathbb{S}^1 \to \mathbb{R}^2$ ; here,  $\mathbb{S}^1$  denotes the unit circle, which is the natural domain of a closed curve, i.e., the start/end point on the curve is arbitrary and is treated as part of nuisance shape variation. Under this representation, there are four different types of nuisance shape variation: translation, scale, rotation and reparameterization. When deriving shape features for classification, we require a distance that is invariant to these four sources of nuisance variability. Unfortunately, it has been documented in the statistical shape analysis literature that the simple  $\mathbb{L}^2$  distance is not invariant to re-parameterization (see e.g. Srivastava et al. (2011)). Mio et al. (2007) instead propose an elastic metric for shape analysis that is invariant to four transformations. including aforementioned re-parameterization; the name "elastic" stems from the interpretability of the metric as measuring changes in stretching and bending as one shape deforms into another.

Unfortunately, the elastic metric is not computable in closed form due to its complicated nature. For efficient implementation of elastic shape analysis, Srivastava et al. (2011) thus propose a simplification via the square-root velocity function transformation as follows. The square-root velocity function (SRVF),  $q:\mathbb{S}^1 \to \mathbb{R}^2$ , of a curve  $\beta$  is defined as  $q=\frac{\dot{\beta}}{\sqrt{|\dot{\beta}|}}$ , where  $\dot{\beta}$  is the derivative of  $\beta$  and  $|\cdot|$  is the Euclidean norm in  $\mathbb{R}^2$ . The space of SRVFs is a subset of  $\mathbb{L}^2$  (Robinson, 2012). Importantly,

under the SRVF representation, the complicated elastic metric simplifies

to the simple  $\mathbb{L}^2$  metric, facilitating efficient shape analysis. Furthermore, nuisance variation due to translation is automatically removed since the SRVF is defined in terms of the derivative of the original curve only. Next, we will build the shape space of curves, using the SRVF representation, by accounting for the remaining sources of nuisance shape variation. In particular, we will consider two different cases of interest in this study: shape only and shape-and-size. We will start with shape-and-size, where the scale of bovid tooth outlines is not treated as nuisance variation (Kurtek et al., 2012). We will then shift to shape only, where scale variation is also removed from the representation. We refer the interested reader to Srivastava and Klassen (2016); Mio et al. (2007); Srivastava et al. (2011); Kurtek et al. (2012); Bharath and Kurtek (2020) for more comprehensive descriptions of these methods.

#### 3.1.1. Size-and-shape features

The pre-size-and-shape space is defined as

$$\mathscr{C} = \left\{ q : \mathbb{S}^1 \to \mathbb{R}^2 \middle| \int_{\mathbb{S}^1} q(t) |q(t)| dt = 0 \right\}.$$

Here,  $\int_{\mathbb{S}^1} q(t)|q(t)|dt=0$  is the closure condition ensuring that statistical analysis treats bovid tooth outlines as closed curves. Next, we will remove variation due to rotations and re-parameterizations from the representation space. First, rotation of a curve  $\beta$  via a rotation matrix  $O \in SO(2) = \{O \in \mathbb{R}^{2 \times 2} \big| O^TO = I, det(O) = 1\}$ , given by  $O\beta$ , results in rotation of its SRVF: Oq. Second, re-parameterization of a curve  $\beta$  via a function  $\gamma \in \Gamma = \{\gamma : \mathbb{S}^1 \to \mathbb{S}^1 \big| \gamma$  is orientation preserving diffeomorphism $\}$ , given by composition  $\beta \circ \gamma$ , results in the following change in its SRVF:  $(q \circ \gamma) \sqrt{\gamma}$ . Then, one can unify all possible rotations and re-parameterizations of the SRVF of a bovid tooth outline via the set

$$[q] = \{ O(q \circ \gamma) \sqrt{\dot{\gamma}} \mid O \in SO(2), \gamma \in \Gamma \}, \tag{1}$$

which is called an equivalence class and is used as a unique representation of the shape-and-size of a bovid tooth outline. The natural shapeand-size distance between two bovid tooth outlines is given by

$$d_{E}([q_{1}], [q_{2}]) = \min_{O \in SO(2), \gamma \in \Gamma} ||q_{1} - O(q_{2} \circ \gamma) \sqrt{\dot{\gamma}}||.$$
 (2)

This is simply the  $\mathbb{L}^2$  distance between  $q_1$  and  $q_2$  after aligning one sizeand-shape to the other by optimizing over rotations and reparameterizations. Implementation details for solving this optimization problem can be found in Srivastava and Klassen (2016). Intuitively, one can think of the distance between size-and-shapes (or shapes) as the amount of deformation needed to go from one size-and-shape to the other.

Fig. 2 demonstrates the benefits of using an elastic distance to quantify size-and-shape differences between bovid tooth outlines, wherein one accounts for rotation and re-parameterization variability, as compared to a non-elastic distance, wherein one accounts for rotation variability but fixes the parameterization to arc-length (as done in elliptical Fourier analysis). The top row shows the elastic size-and-shape deformation between two Alcelaphini specimens in this study, while the bottom row shows the non-elastic deformation. Notice that, in the top row, in the upper right portion of the tooth the indent is better maintained throughout the path. On the other hand, in the bottom row, this

Table 2
Sample sizes for each tooth type, i.e. Lower Molar (LM) and Upper Molar (UM) 1, 2 and 3, and tribe.

Type	Alcelaphini	Antilopini	Bovini	Hippotragini	Neotragini	Reduncini	Tragelaphini
LM1	136	42	25	86	127	123	101
LM2	145	47	26	82	127	131	95
LM3	131	47	24	79	120	121	97
UM1	125	40	25	95	129	119	112
UM2	129	40	26	97	133	119	113
UM3	130	40	24	93	115	123	99





Fig. 1. Example of a color photo (left) and black and white image (right) from the B.O.V.I.D. database. The specimen is an upper second molar (UM2) Alcelaphus buselaphus, National Museum Bloemfontein (NMB) 12264.

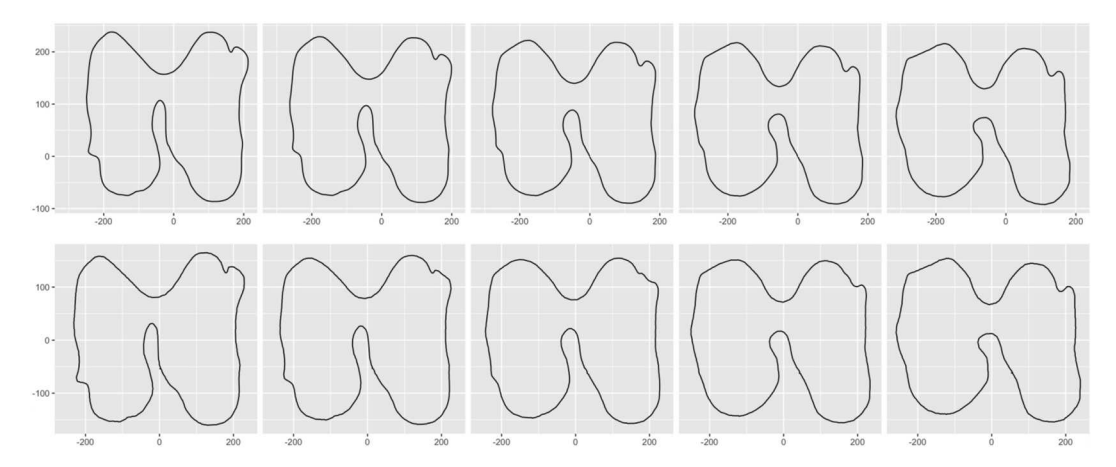


**Fig. 2.** Paths of minimal shape deformation between two teeth from *A. buselaphus*: DSCN 2871 and DSCN4796. The deformation in the top row was generated using elastic size-and-shape analysis while the bottom row presents a non-elastic deformation (parameterization fixed to arc-length).

notch vanishes almost entirely in the middle of the deformation. Thus, the elastic size-and-shape deformation between these two specimens is more natural than the non-elastic one.

The size-and-shape distance defined in Equation (2) can be used to define a sample mean size-and-shape as follows. Let  $\beta_1, ..., \beta_n$  denote a sample of bovid tooth outlines, and  $q_1, ..., q_n$  their corresponding SRVFs. The sample mean is given by

$$\widehat{\mu} = \underset{q \in \mathscr{E}}{\operatorname{argmin}} \sum_{i=1}^{n} d_{E}([q], [q_{i}])^{2}. \tag{3}$$

The sample mean estimate can then be used to estimate the size-and-

shape covariance and carry out principal component analysis (PCA). First, let  $\nu_i = q_i^* - \widehat{\mu}, i = 1,...,n$ , where each  $q_i^* = O_i^*(q_i \circ \gamma_i^*) \sqrt{\dot{\gamma}_i^*}$  and  $(O_i^*, \gamma_i^*) = \underset{O \in SO(2), \gamma \in \Gamma}{\operatorname{argmin}} \|\widehat{\mu} - O(q_i \circ \gamma) \sqrt{\dot{\gamma}}\|$ . Assuming that each size-and-shape  $q_i^*$  is sampled with N points (in our implementation, we use N = 100), each  $\nu_i$  is a vector in  $\mathbb{R}^{2N}$  after stacking of the x and y coordinates. Then, the sample size-and-shape covariance is given by  $K = \frac{1}{n-1} \sum_{i=1}^n \nu_i \nu_i^T$ . To perform PCA, the covariance matrix is decomposed as  $K = U \Sigma U^T$ , where the columns of the orthonormal matrix U contain the primary directions of size-and-shape variation and the diagonal elements of the diagonal matrix  $\Sigma$  contain the corresponding variances. Dimension reduction of the size-and-shape data can be achieved by computing PC coefficients

(lower-dimensional Euclidean coordinates of size-and-shape) as  $c_i$ 

 $\{v_i^T U_j, j=1,...,n-1\}$ . An example of size-and-shape PCA analysis for bovid teeth from the Alcelaphini tribe is shown in Fig. 3. We display the first three primary directions of size-and-shape variation in each row sampled at -1.5, -1, -0.5, 0 (size-and-shape average in red), 0.5, 1, 1.5 standard deviations.

The vectors  $v_1, ..., v_n$ , as well as the PC coefficient vectors  $c_1, ..., c_n$  generated from them, can be used as features in classification models. The vectors and PC coefficients are computed using two different methods resulting in four total scenarios of feature generation:

- 1. Overall (OV). The bovid tooth outlines are pooled across classes and the overall size-and-shape mean  $\widehat{\mu}$  is computed. Each size-and-shape  $q_i^*$  (aligned to the pooled mean  $\widehat{\mu}$ ) is transformed into the vector  $v_i = q_i^* \widehat{\mu}$ . Number of features: 200.
- 2. Individual (I). Bovid tooth outlines within each class g are used to compute individual size-and-shape means  $\widehat{\mu}_g$ . Each size-and-shape  $q_i^*$  is registered to each class mean  $\widehat{\mu}_g$  and transformed into the vector  $\nu_{ig}$ . Then, the vectors  $\nu_{ig}$ , g=1,...,G, are used as features. Number of features:  $G \times 200$ .
- 3. PC Overall (OV-PC). This approach is the same as OV, but with an additional step of dimension reduction to size-and-shape PC coefficients. Number of features: n-1.

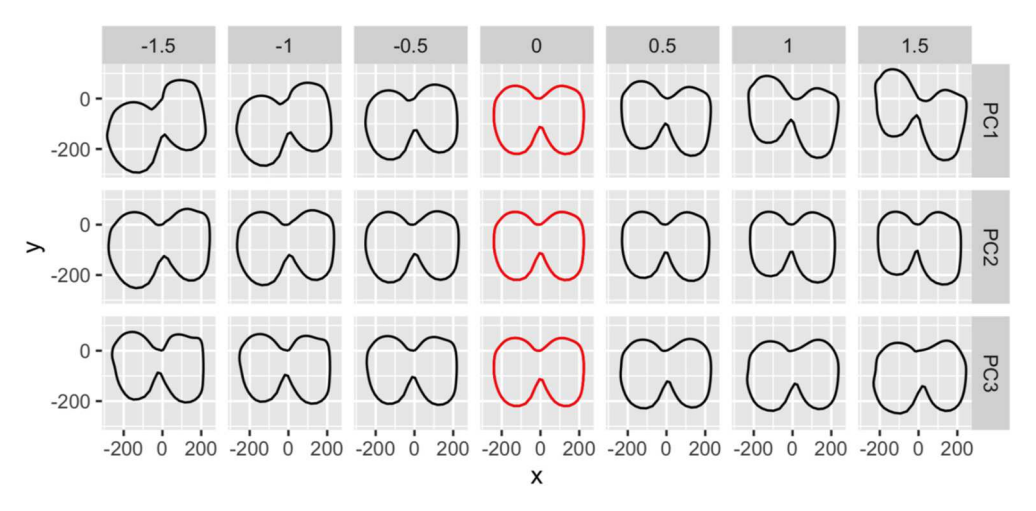


Fig. 3. The three primary PC directions of variation (top row to bottom row) for teeth from the Alcelaphini tribe. The mean size-and-shape is shown in red in each row. The three shapes to the left and right of the mean show size-and-shapes that are 0.5, 1, and 1.5 standard deviations from the mean in the negative and positive direction, respectively.

4. Individual (I-PC): This approach is the same as I, but with an additional step of dimension reduction to size-and-shape PC coefficients for each class g. Number of features:  $G \times (n-1)$ .

The set of generated size-and-shape features will generically be denoted by X and indexed with a superscript when necessary to distinguish which method of feature generation was used (e.g.  $X^{OV}$ ,  $X^I$ , etc.).

#### 3.1.2. Shape features

Feature generation based on shape only proceeds in similar fashion to the size-and-shape case with a few modifications. Throughout this section, we use the same notation as in the previous one. The pre-shape space is defined as

$$\mathscr{C} = \left\{ q : \mathbb{S}^1 \to \mathbb{R}^2 \middle| \int_{\mathbb{S}^1} q(t) |q(t)| dt = 0, ||q||^2 = 1 \right\}.$$

The second constraint restricts attention to unit length curves, and the pre-shape space is now a subset of the unit sphere in  $\mathbb{L}^2$ . The shape of a bovid tooth outline is again defined via an equivalence class as given in Equation (1). Due to the unit length constraint, the shape distance is defined using the shortest great circle arc on  $\mathscr{C}$  as

$$d_{E}([q_{1}],[q_{2}]) = \min_{O \in SO(2), \gamma \in \Gamma} \cos^{-1} \left( \left\langle q_{1}, O(q_{2} \circ \gamma) \sqrt{\dot{\gamma}} \right\rangle \right),$$

where  $\langle \cdot, \, \cdot \rangle$  is the  $\mathbb{L}^2$  inner product.

Given bovid tooth outlines  $\beta_1, ..., \beta_n$ , with corresponding SRVFs  $q_1, ..., q_n$ , the shape distance can be used to define the sample mean shape  $\widehat{\mu}$  in the same fashion as in Equation (3). Since  $\mathscr C$  is a non-linear space, PCA is carried out in a local linear approximation called the tangent space. In particular, each shape  $q_i^* = O_i^*(q_i \circ \gamma_i^*) \sqrt{\hat{\gamma}_i^*}$ , where  $(O_i^*, \gamma_i^*) =$ 

 $\underset{0 \in SO(2), \gamma \in \Gamma}{\operatorname{argmin}} \| \widehat{\mu} - O(q_i \circ \gamma) \sqrt{\widehat{\gamma}} \|, \text{ is transformed into a vector } \nu_i \text{ in the linear }$ 

tangent space at the shape mean  $\hat{\mu}$  using the inverse-exponential map, which is closely related to the defined shape distance  $d_E$ :

$$v_i = \exp_{\widehat{\mu}}^{-1} \left( q_i^* \right) = \frac{\eta_i}{\sin(\eta_i)} \left( q_i^* - \cos(\eta_i) \widehat{\mu} \right),$$

where  $\eta_i = d_E([\widehat{\mu}], [q_i])$ . PCA is then carried out in this tangent space using  $v_i$  and the same procedure as described in Section 3.1.1.

Just as with size-and-shape, the shape only derived vectors  $v_1, ..., v_n$  and the PC coefficients  $c_1, ..., c_n$  can be used as features in classification models. We use the same four settings for feature generation: OV, I, OV-PC, and I-PC.

### 3.1.3. Elliptical Fourier analysis (EFA) features

In past studies, bovid tooth shape classification was performed using features generated via elliptical Fourier analysis (EFA) (Matthews et al., 2018). As described earlier, this method requires the bovid tooth outlines to be parameterized with respect to arc-length. We briefly describe this approach to feature generation and include it in our study as a baseline to compare the classification performance using features derived via the elastic shape (-and-size) analysis framework.

EFA decomposes closed curves into a series of ellipses. As before, let  $\beta: \mathbb{S}^1 \to \mathbb{R}^2$  denote an absolutely continuous, parameterized closed curve representing the outline of a bovid tooth. Further, let  $\beta_x$  and  $\beta_y$  represent the x and y coordinate functions of  $\beta$ . Then, EFA applies the following decomposition to  $\beta_x$  and  $\beta_y$ :

$$\beta_x(t) = A_0 + \sum_{h=1}^{H} a_h \cos(ht) + \sum_{h=1}^{H} b_h \cos(ht)$$
, and

$$\beta_{y}(t) = C_{0} + \sum_{h=1}^{H} c_{h} \cos(ht) + \sum_{h=1}^{H} d_{h} \cos(ht),$$

where H is the number of harmonics used,  $A_0$  and  $C_0$  are constants, and  $a_h$ ,  $b_h$ ,  $c_h$ ,  $d_h$  are the amplitudes associated with the h-th harmonic. The collection of these amplitudes, as well as principal components derived from them, can then be used as input features for classification methods. The full set of EFA amplitudes and principal components is denoted by  $\mathbf{X}^{EFA}$ ; the number of features in  $\mathbf{X}^{EFA}$  is  $4 \times H +$  number of PCs. In this particular study, H = 15 with 30 PCs resulting in 90 total features. EFA with and without scale normalization are both considered here to compare to the elastic size-and-shape and shape only settings. EFA was implemented using the efourier function in the package Momocs (Bonhomme et al., 2014) in R (R Core Team, 2021).

## 3.2. Classification

The features, whose generation methods were described in the preceding sections, are then used as predictors in machine learning classifiers. Regardless of the features used, we are interested in classification at two taxonomic levels: tribe and species.

Specifically, we are interested in estimating the following probabilities

$$\pi(y_i^t = g^t | \mathbf{X})$$
 and  $\pi(y_i^s = g^s | \mathbf{X})$ ,

where  $y_i^t$  and  $y_i^s$  are the tribe and species labels for the *i*-th observation,

 $g^t = 1, ..., G^t$  and  $g^s = 1, ..., G^s$ ,  $G^t$  and  $G^s$  are the number of unique tribes and species, respectively, and **X** is a set of features derived from one of the methods described in the preceding sections.

Tribe modeling is performed directly using a training dataset of bovid tooth outlines and the corresponding tribe memberships. However, since species are nested within tribes, species classification modeling is performed conditionally on tribe. Specifically, we aim to estimate

$$\pi(y_i^s = g^s | X) = \pi(y_i^s = g^s \cap y_i^t = g^t | X) = \pi(y_i^s = g^s | y_i^t = g^t, X) \pi(y_i^t = g^t | X),$$

where the superscripts s and t denote species and tribe, respectively. In practice, this means that we must fit  $G^t+1$  classification models: one model for species classification conditional on each tribe  $g^t=1, ..., G^t$ , and one model for tribe classification. Note that when performing classification of the species, we use the means of *tribes* (and not species) to define the feature sets X. This is done for two main reasons: (1) there are 20 species as opposed to only seven tribes resulting in higher computational efficiency, and (2) the sample size in each species class tends to be very small.

The three machine learning classification methods considered in this study were random forests (RF) (Ho, 1995; Breiman, 2001), support vector machines with a linear kernel (SVM-L) and support vector machines with a radial kernel (SVM-R) (Cortes and Vapnik, 1995).

Random forest uses a collection of classification trees to generate a final class prediction. Each tree produces its own classification decision and is estimated using a bootstrapped sample of the data. The resulting collection of decisions is then pooled together to obtain a final classification decision based on the forest of trees. In this work, we used the default values of the parameters provided by the randomForest package (Liaw and Wiener, 2002). Specifically, each forest contained 500 trees and the number of variables randomly sampled at each split was the square root of the number of available features. No additional hyperparameters were tuned during the training stage.

SVMs perform classification by constructing linear boundaries in the feature space. However, since it is often difficult to find good boundaries in the original feature space, a transformed feature space is often

considered. Different transformations of the feature space are generated in practice by choosing different kernel functions. We consider both a linear and a radial kernel. In both cases, during the training stage, the cost parameter C is tuned over a grid of values ranging from  $10^{-1}$  to  $10^{3}$ . In addition, in the SVM with a radial kernel, the parameter  $\gamma$  which controls the spread of the kernel is tuned over a grid of values from  $10^{-3}$  to  $10^{3}$ .

Further details about the random forest and SVM classifiers can be found in James et al. (2023). All classification was performed in the R programming language (R Core Team, 2021), with random forests implemented using the R package randomForest (Liaw and Wiener, 2002) and SVMs implemented using the R package e1071 (Meyer et al., 2023). Classification performance is always estimated using five-fold cross validation, i.e., four folds are used for training the machine learning model with one fold used for testing. The final evaluation of classification performance is an average across the five testing folds.

#### 4. Tribe and species classification results

We report and describe tribe and species classification results based on shape and size-and-shape features separately. In each case, we consider five different types of feature sets, (1) EFA, (2) I, (3) OV, (4) OV-PC and (5) I-PC, and three different types of classification models, (1) RF, (2) SVM-L and (3) SVM-R. hroughout this section, we use five-fold cross-validation to compute classification performance.

#### 4.1. Tribe classification: shape features

Fig. 4 shows results of classifying bovid tooth outlines at the tribe level, stratified by tooth type, using shape features. Nearly uniformly, SVM-R yields the highest classification accuracy. These findings are similar to those reported in Matthews et al. (2018), which also identified SVM-R as the best classification method when using EFA features. Overall, RF classification performance is almost completely dominated by SVM-L and SVM-R performance.

When comparing across different feature generation approaches, method I, based on elastic shape analysis, tends to yield the highest

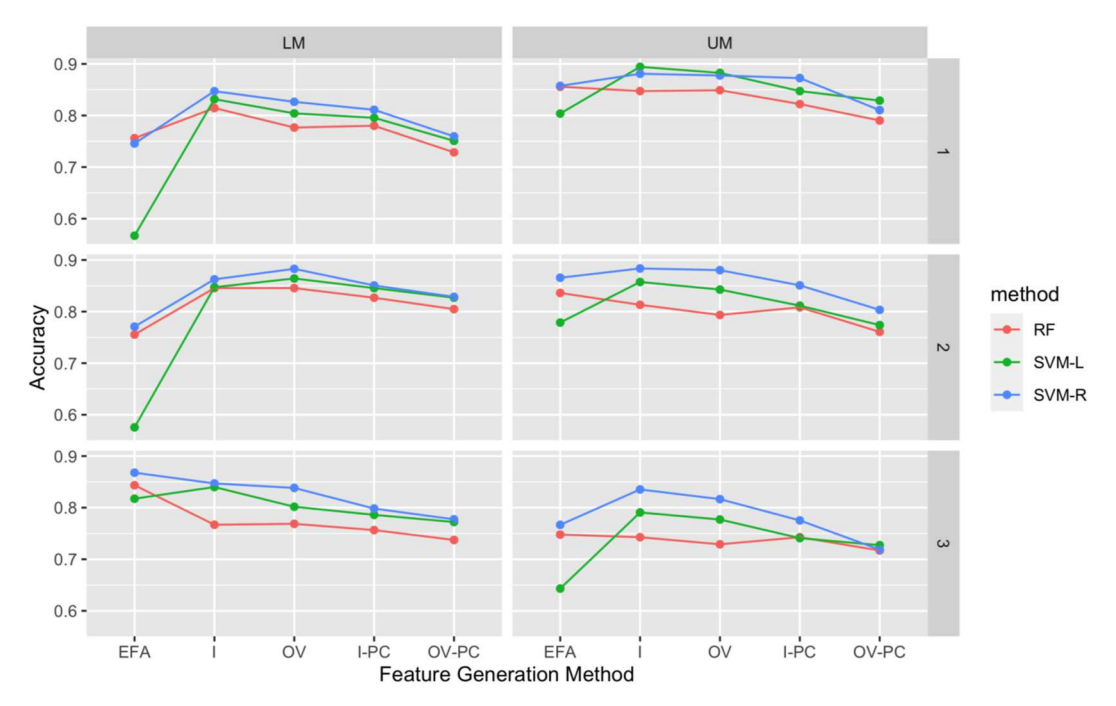


Fig. 4. Shape Features: Tribe classification accuracy for six different tooth types (LM1, LM2, LM3, UM1, UM2, UM3) based on five different methods of feature generation (EFA, I, OV, I-PC, OV-PC) and three classification models (RF, SVM-L, SVM-R). Note that EFA generates non-elastic shape features while the other four are feature sets derived using elastic shape analysis.

classification accuracy. For SVM-R, method I yields the highest accuracy for four out of the six tooth types. Further, SVM-R using method I for feature generation is the only classification method with accuracy above 80% for all tooth types (LM1: 84.7%, LM2: 86.2%, LM3: 84.7%, UM1: 88.1%, UM2: 88.4%, UM3: 83.5%). Comparing methods I and OV, method I generally, though not always, yields slightly higher classification accuracy. Exceptions include classification for LM2, where OV performs as well as or better for all three methods considered here (RF-I: 84.6% vs. RF-OV: 84.6%, SVM-L-I: 84.7% vs. SVM-L-OV: 86.4%, SVM-R-I: 86.2% vs. SVM-R-OV: 88.3%), and random forest for UM1 (RF-I: 84.7% vs. RF-OV: 84.9%) and LM3 (RF-I: 76.7% vs. RF-OV: 76.9%). While this is not surprising since method I generates a larger feature set than method OV, the observed performance differences are small. The methods I-PC and OV-PC, which use PC coefficients as features, generally perform worse than their non-PC counterparts I and OV. Finally, EFA features yield highly variable performance across classification models and tooth types. In most cases, EFA feature-based classification accuracy is lower than classification accuracy via features generated using elastic shape analysis. However, for LM3, EFA features perform quite well (RF-EFA: 84.3%, SVM-L-EFA: 81.7%, and SVM-R-EFA: 86.87%) and tend to outperform elastic shape analysis-based features. Based on the totality of these results, we conclude that the best classification accuracy is attained by SVM-R with shape features generated using method I.

While tribe classification accuracy is generally greater than 80% and often near 90%, it is not uniform across different tribes and tooth types. Fig. 5 shows the classification accuracy for each tribe when using SVM-R as the classification model with features generated via method I. Tribe Alcelaphini appears to be the easiest to classify, with classification accuracy at or above 94% across all tooth types (ranging from 94.1% for LM1 to 99.1% for UM1). Classification performance for tribes Neotragini and Tragelaphini is also very good across all tooth types, with accuracies generally falling between 85% and 90% with the exception of UM2 (Neotragini: 94%, Tragelaphini: 91.5%). Classification accuracy for the other four tribes behaves differently with much more variation across the six tooth types; the worst performances were observed in Bovini (UM2: 38.5% sample size of 26; LM3: 62.5%, sample size of 24; UM3: 62.5%, sample size of 24; UM1: 64%, sample size of 25), Hippotragini (LM3: 61.5%), and Antilopini (UM3: 63.3%). However, it is notable that

tribe Bovini has the smallest sample size across all tribes. We additionally provide ROC curves in Fig. 6, which can be used for a detailed assessment of specificity and sensitivity across the seven tribes. As before, we use SVM-R as the classification model with method I to generate shape features.

#### 4.2. Tribe classification: size-and-shape features

Fig. 7 displays classification results at the tribe level stratified by tooth type based on size-and-shape features. As expected, including tooth size information as part of the feature generation process improves classification accuracy. As in the case of shape features, it appears that size-and-shape features from elastic shape analysis generally outperform EFA-based non-elastic features. This provides further evidence for the value in using elastic shape analysis to generate features for classification. Interestingly, in this case, OV-PC features generally yield highest classification accuracies across classification models and tooth types. Further, RF is much more competitive as compared to SVM-L and SVM-R. Pooling results across all six tooth types, RF with OV-PC features classified 3350 out of 3838 teeth correctly (87.29%); using shape features only, 2675 out of 3838 (69.70%) teeth were classified correctly using RF with OV-PC features. This is quite different from what was observed when shape features, without size information, were used for classification; SVM-R with features generated using method I generally performed the best (SVM-R-I: 86.0%).

Fig. 8 shows classification accuracy across different tribe and tooth types. As before, classification rates corresponding to tribes Alcelaphini (LM1: 95.8%, LM2: 98.4%, LM3: 99.2%, UM1: 98.2%, UM2: 94.9%, UM3: 91.7%) and Bovini (LM1: 52.0%, LM2: 73.1%, LM3: 79.2%, UM1: 28.0%, UM2: 19.2%, UM3: 16.7%) are generally the highest and lowest, respectively. Notably, size-and-shape features yield a considerable improvement in classification accuracy for tribe Hippotragini, which is the tribe containing the largest tooth size on average. Based on shape features generated via method I and using SVM-R, classification rates were as high as 84.5% for UM2 and as low as 61.5% for LM3. Incorporating size information improved classification accuracy of Hippotragini to a low of 78.5% for UM3 and a high of 93.7% for UM1. Additionally, with the exception of Bovini, all tooth types and tribes have classification rates above 75%, which was not the case when only

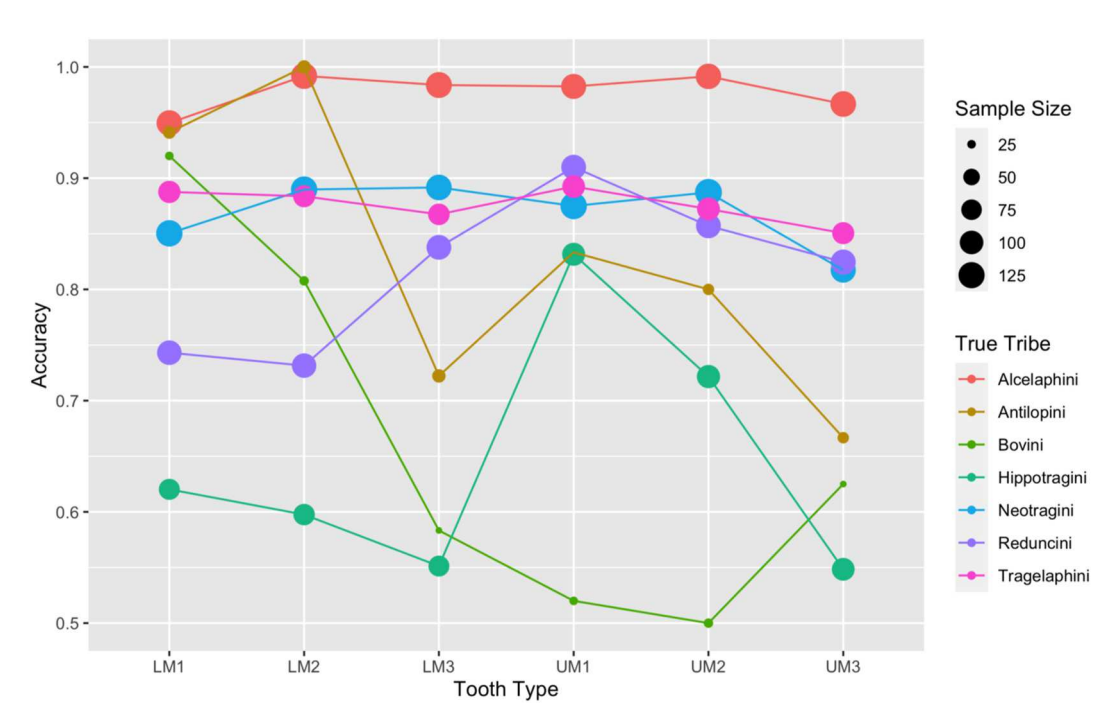


Fig. 5. Shape Features: Tribe classification accuracy, stratified by different tribes, using SVM-R as the classification model and method I for shape feature generation.

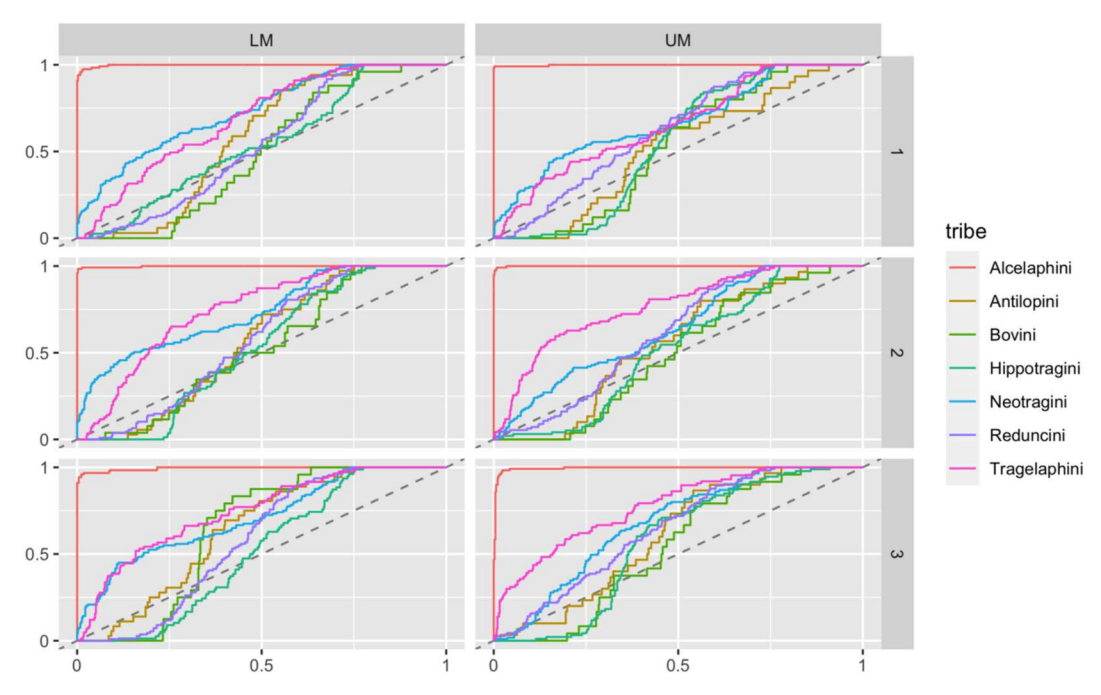


Fig. 6. Shape Features: ROC curves for tribe classification for six different tooth types (LM1, LM2, LM3, UM1, UM2, UM3), using SVM-R as the classification model and method I for shape feature generation.

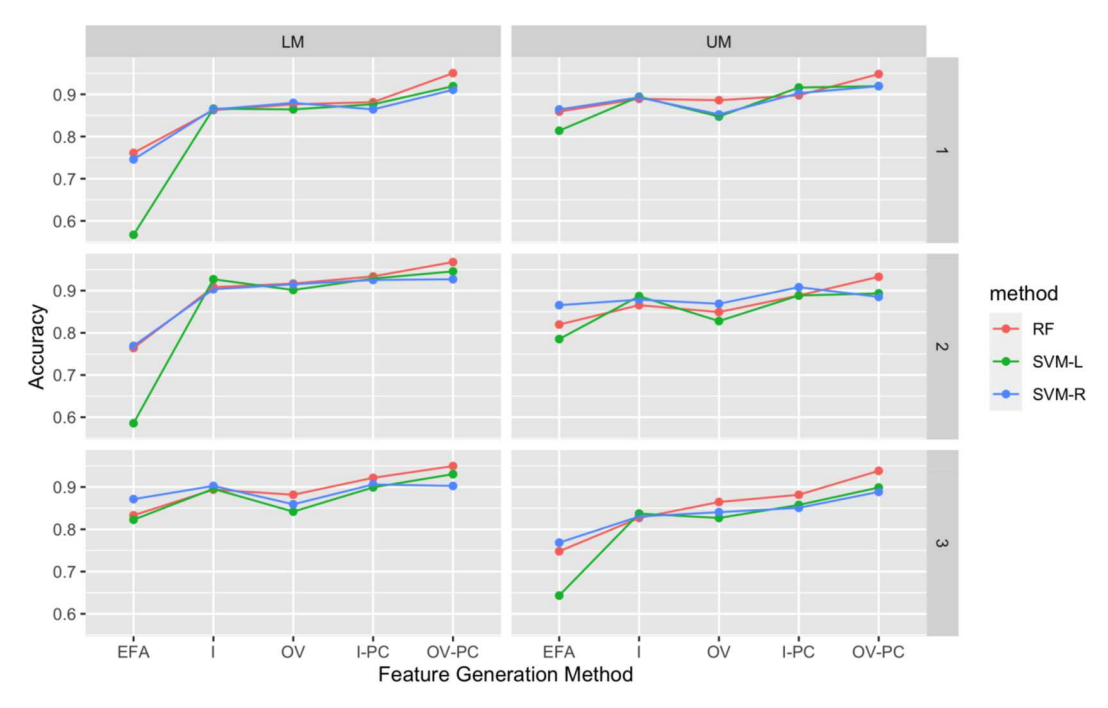


Fig. 7. Size-and-shape Features: Tribe classification accuracy for six different tooth types (LM1, LM2, LM3, UM1, UM2, UM3) based on five different types of feature generation (EFA, I, OV, I-PC, OV-PC) and three classification models (RF, SVM-L, SVM-R). Note that EFA generates non-elastic size-and-shape features while the other four are feature sets derived using elastic shape analysis.

shape features were used for classification. We also provide ROC curves in Fig. 9 for each of the seven tribes. As before, we use SVM-R as the classification model with method I to generate shape features.

## 4.3. Species classification: shape features

We repeated all classification experiments at the species level. Given the larger number of species relative to tribes (20 vs. 7), we expect lower classification rates in this case than what was seen for tribe classification. Based on Fig. 10, we observe similar patterns when classifying species to those we saw for tribe classification. SVM-R with shape features generated using method I attains the highest classification accuracy for three out of the six tooth types (LM1, UM2 and UM3); this is the only combination of classification model and feature generation method that yields classification rates above 65% for all tooth types (LM1: 69.9%, LM2: 71.0%, LM3: 68.7%, UM1: 72.3%, UM2: 71.9%, UM3: 66.7%). Similar to the tribe classification experiments, features generated using elastic shape analysis tend to outperform EFA-based non-elastic features.

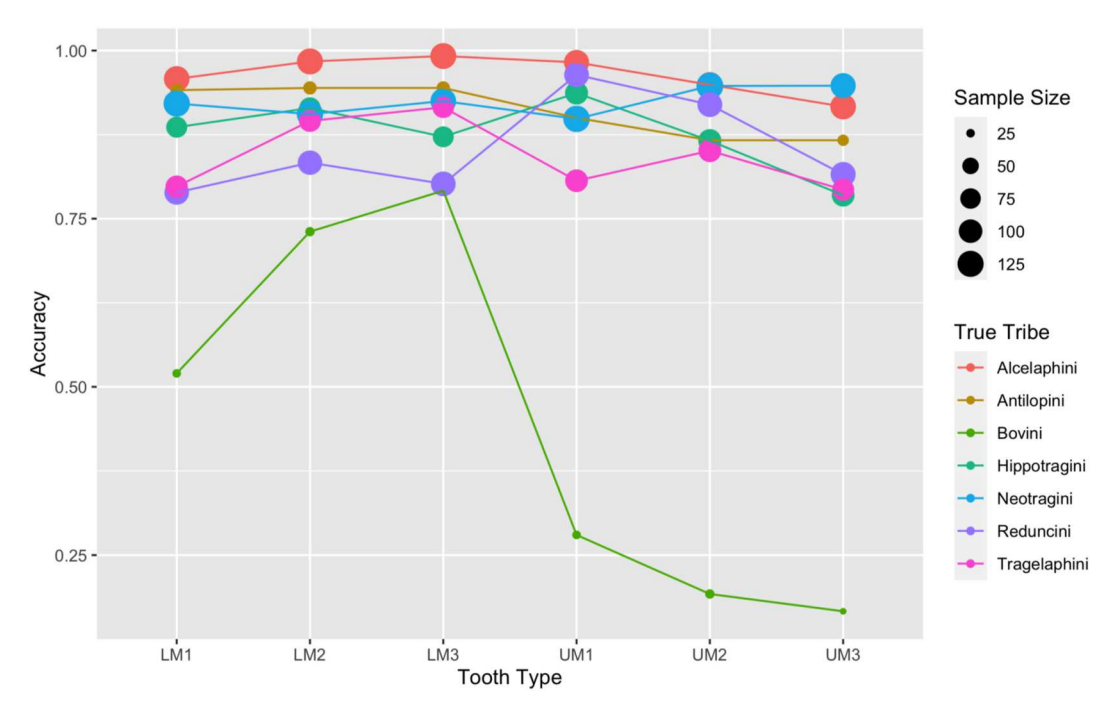


Fig. 8. Size-and-shape Features: Tribe classification accuracy, stratified by different tribes, using SVM-R as the classification model and method I for feature generation.

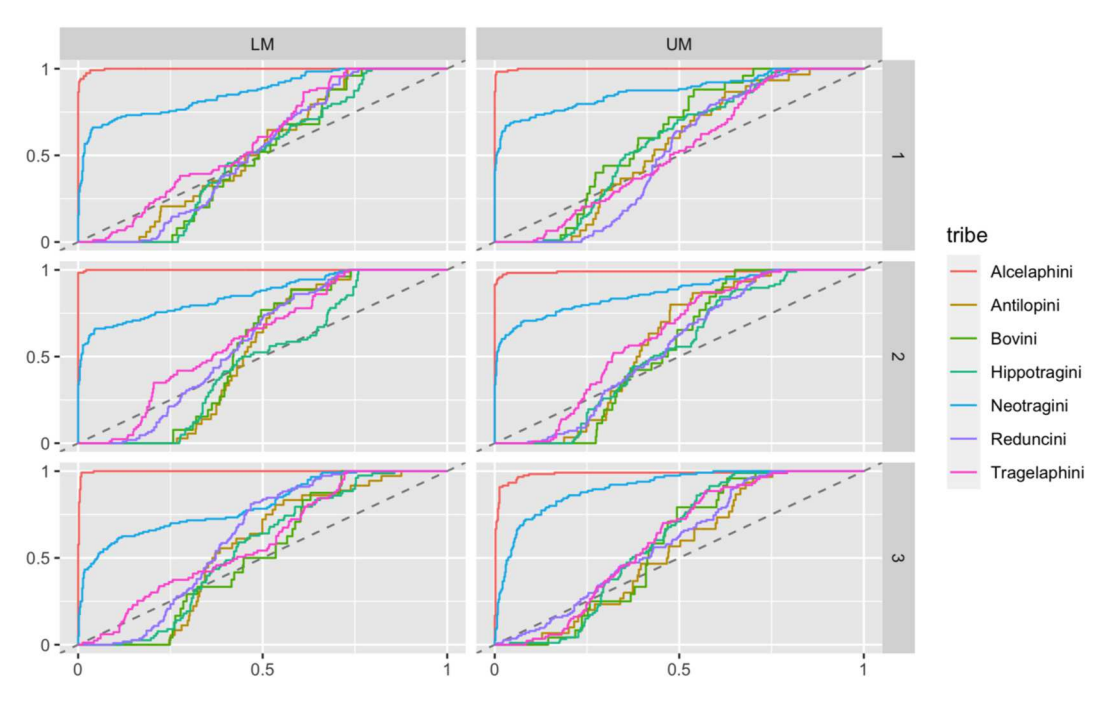


Fig. 9. Size-and-shape Features: ROC curves for tribe classification for six different tooth types (LM1, LM2, LM3, UM1, UM2, UM3), using SVM-R as the classification model and method I for size-and-shape feature generation.

## 4.4. Species classification: size-and-shape features

Fig. 11 displays species classification accuracy when size-and-shape features are used. As in the case of tribe classification, we observe a general improvement across tooth types when preserving size information in feature generation. For example, the overall species classification accuracy with SVM-R and feature generation method I using shape versus size-and-shape features improved from 70.1% to 75.7%. The difference is even more pronounced when using the best performing species classification model: RF with feature generation method OV-PC.

In this case, the classification rate based on shape features was 56.7% whereas using size-and-shape information yields a classification accuracy of 88.5%. Not only is the RF with features generated using OV-PC the best overall, it is also the best in terms of accuracy in all 6 tooth types (LM1: 88.8%, LM2: 91.2%, LM3: 87.3%, UM1: 88.6%, UM2: 87.2%, UM3: 88.0%). Another notable observation in the results for size-and-shape vs size is that when using size-and-shape, the feature generation methods using PC's (i.e. OV-PC and I-PC) perform better in terms of accuracy than the non-PC based procedures (EFA: 62.7%, I: 77.7%, OV: 77.1%, I-PC: 81.7%, OV-PC: 88.5%). This is the opposite of what

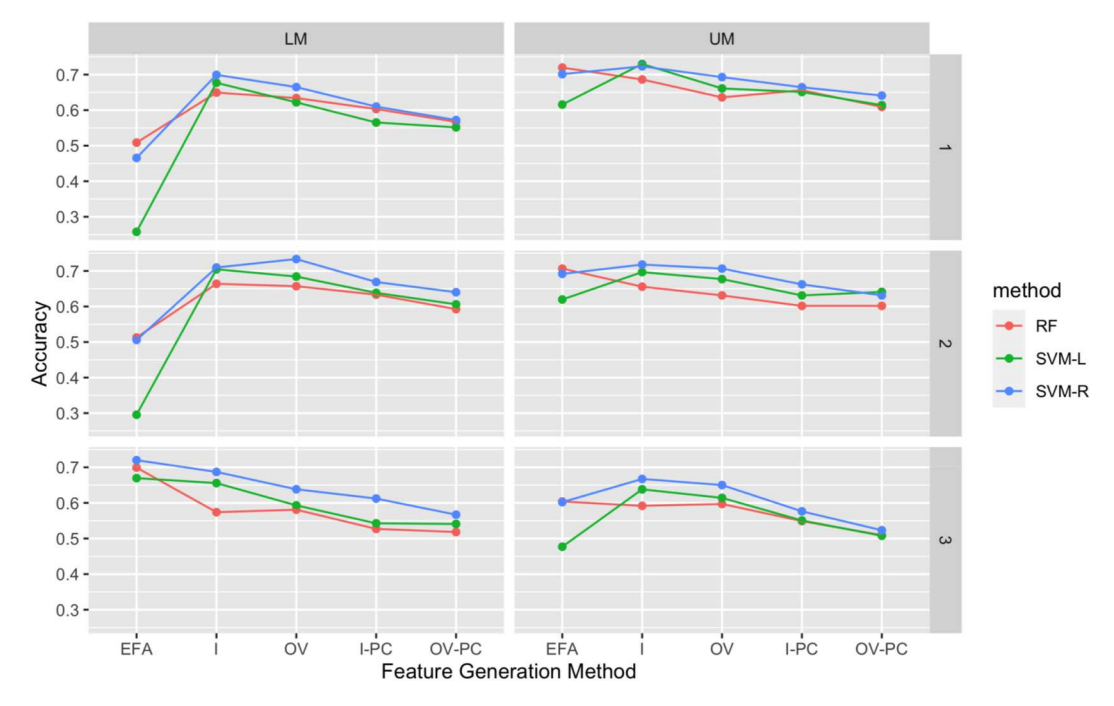


Fig. 10. Shape Features: Species classification accuracy for six different tooth types (LM1, LM2, LM3, UM1, UM2, UM3) based on five different types of feature generation (EFA, I, OV, I-PC, OV-PC) and three classification models (RF, SVM-L, SVM-R). Note that EFA generates non-elastic size-and-shape features while the other four are feature sets derived using elastic shape analysis.

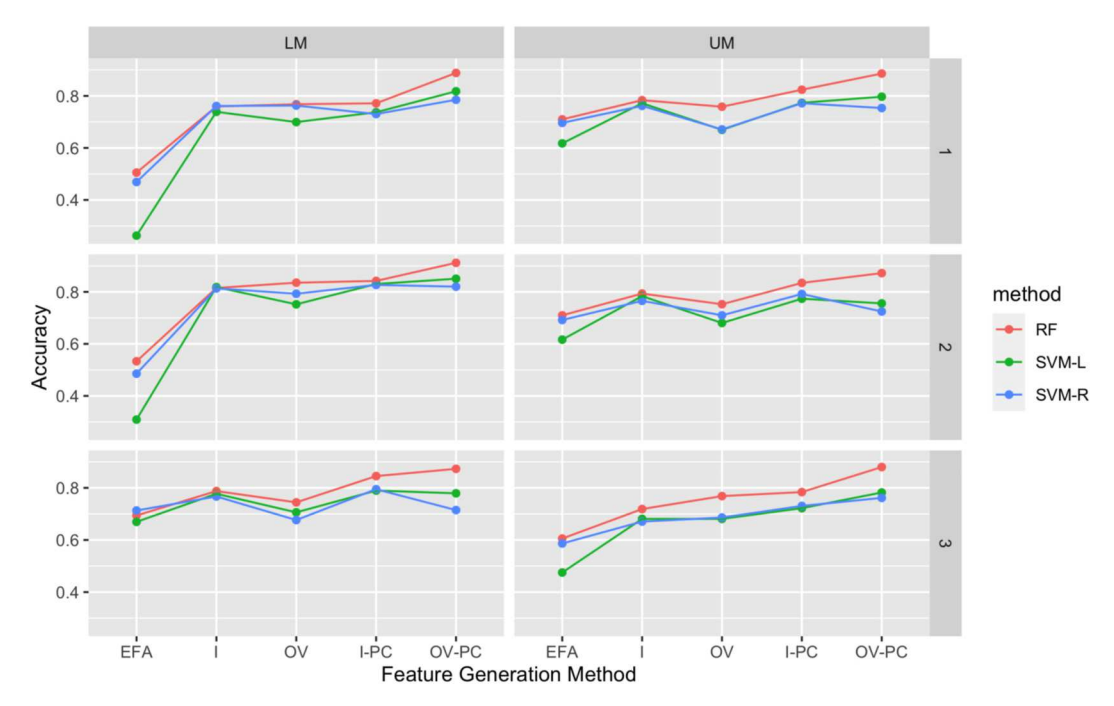


Fig. 11. Size-and-shape Features: Species classification accuracy for six different tooth types (LM1, LM2, LM3, UM1, UM2, UM3) based on five different types of feature generation (EFA, I, OV, I-PC, OV-PC) and three classification models (RF, SVM-L, SVM-R). Note that EFA generates non-elastic size-and-shape features while the other four are feature sets derived using elastic shape analysis.

was observed when using shape only.

Finally, as seen throughout the classification experiments, nonelastic EFA-based features generally yield worse classification accuracy than the elastic shape analysis-based features.

## 5. Reclassification of Gladysvale alcelaphines

In the previous sections, we found that the SVM-R classification

model with shape or size-and-shape features generated using the I and OV methods performed well in the tribe and species classification tasks. We now use these methods for classification of medium-sized alcelaphine teeth recovered from GVED. We report classifications at the tribe and species level for both shape and size-and-shape generated features. For each specimen, the probability of belonging to each taxa was estimated and each tooth was classified to the taxa with the highest probability.

Table 3 shows the number of different fossil tooth types considered in this study. With 12 out of 32 (37.5%) of our fossil specimens, the most common tooth type in this sample is the third lower molar (LM3). The second upper molar (UM2) is the least common tooth type with only 2 out of 32 (6.25%). Overall, our sample includes 21 lower molars and 11 upper molars.

We use the same data as in previous sections to generate shape and shape-and-size feature sets using the I and OV methods. The features are then used to train an SVM-R classifier. We also generate the same types of features for the 32 fossils and use them in the trained SVM-R classification model to predict their tribe and species. We consider shape and shape-and-size separately.

#### 5.1. Reclassification with shape features

Table 4 lists the reclassifications of the medium sized alcelaphines from GVED using shape features. In their original classification, these teeth were determined to all likely be alcelaphines, and so it is expected that the most common predicted tribe should be Alcelaphini. Indeed, that is what is observed. Using shape features generated via method I, 27 of the 32 (84.38%) fossil teeth were classified as Alcelaphini. Using OV-based features, 26 out of 32 (81.25%) of the fossil teeth were classified as Alcelaphini. Recall that method I outperformed method OV in the previous tribe classification experiments, which is also consistent with what is observed here. When fossil teeth were not classified as Alcelaphini, they were most commonly classified as Hippotragini (6.25% and 9.38% for methods I and OV, respectively). No teeth were classified to either Bovini or Antilopini with method I, and with method OV no teeth were classified to Bovini. This could be the result of the much lower training sample sizes in these two tribe classes.

Table 5 shows the species level classifications of the GVED teeth using shape features. Most of the teeth were classified as one of the four species in Alcelaphini, as expected. Four other species are represented including *Oryx gazella*, *Ourebia ourebi*, *Taurotragus oryx*, and *Tragelaphus scriptus*. Note that the total number of teeth classified to each tribe is not consistent across Tables 4 and 5 This is due to the fact that the teeth were classified to a tribe or species based on the highest probability. Thus, a tooth could have the highest probability of belonging to a tribe, but the highest species probability does not necessarily need to belong to that same tribe, though in a vast majority of cases it did.

## 5.2. Reclassification with size-and-shape features

Table 6 provides tribe level fossil reclassification results when size-and-shape features are used. Using both size and shape is more informative when trying to identify teeth in the fossil record. 31 of the 32 teeth were identified as Alcelaphini when features were generated using method I; 28 of the 32 teeth were identified as Alcelaphini when features were generated using method OV. When size-and-shape features were used to identify species, one specimen was identified as *D. dorcas*, 15 as A *buselaphus*, 7 as C *gnou* and 6 as C *taurinus*. The results of the study increase the number of *D. dorcas* and *C. taurinus* identified and add the alcelaphines *A. buselaphus* and *C. gnou* (Tables 4 and 6; Lacruz et al. (2002)). These species are not atypical for the area. The aforementioned article identified *Connochaetes* sp. indet. According to Brink (2005), *C. taurinus* and *C. gnou* can be difficult to identify based on isolated teeth especially since they were closer in size in the past. In addition, *C. gnou* 

**Table 3**Breakdown of tooth type for the 32 Gladysvale fossils. LM and UM are lower and upper molars, respectively.

	LM	UM
1	5	3
2	4	2
3	12	6

**Table 4**Shape Features: Tribe level classifications of the Gladysvale fossil teeth using shape features generated via elastic shape analysis (I and OV) and classification method SVM-R.

Method	Type	Alcelaphini	Hippotragini	Neotragini	Tragelaphini
I	LM1	2	1	0	2
	LM2	4	0	0	0
	LM3	11	0	1	0
	UM1	2	0	1	0
	UM2	2	0	0	0
	UM3	6	0	0	0
	Total	27	1	2	2
OV	LM1	1	2	0	2
	LM2	3	1	0	0
	LM3	11	0	1	0
	UM1	3	0	0	0
	UM2	2	0	0	0
	UM3	6	0	0	0
	Total	26	3	1	2

was recovered from the site of Cornelia-Uitzoek, an older site in the Free State Province which dates to 1.07–0.99 Ma (Brink, 2005; Brink et al., 2012) and from a geographically closer site in the Gauteng Province. Haasgat, dating to at least the mid-to late-Pleistocene (Adams, 2012). Alcelaphus buselaphus was identified from the internal Gladysvale deposits in the original announcement paper by Berger et al. (1993) but not from the younger GVED deposits (Lacruz et al., 2002). The first appearance date for this taxa is from Bodo Locality 1, Ethiopia at 0.6 Ma (Vrba, 1997). In South Africa, this taxa was recovered from the site of Florisbad which dates to 300-100 Ka. in the Free State (Brink, 1987) but not in the Gauteng Province until 88-62 Ka at Plovers Lake (Brophy et al., 2014). However, other researchers have identified medium-sized alcelaphines from older sites in Gauteng that could potentially be A. buselaphus (e.g. (de Ruiter et al., 2008; Vrba, 1997)). Regardless, the recognition of this taxa in the Gladysvale external deposits would push back the first appearance date in the Gauteng Province.

Lacruz et al. (2002) found an NISP and MNI of 1 cf *Oryx gazella* while this study identified an NISP and MNI of 2 teeth as *O. gazella*. These teeth have an incipient goat fold which is consistent with Hippotragini and *O. gazella* (Gentry and Gentry, 1978b, 1978a). Contrary to Gentry and Gentry (1978b,a), basal pillars are variable on mandibular Hippotragini teeth (Brophy and Matthews, 2022) so their absence is not an issue.

Specimen GV8654 reclassified as a Tragelaphini and *Tragelaphus strepsiceros* (Fig. 12). The outline of this tooth resembles a tragelaphine in that it has a strong separation between the lobes and an outgrowth on the distal side of the protocone (mesial lobe), possibly the incorporation of a small basal pillar. Regardless of the outline, the tooth exhibits characteristics consistent with alcelaphines including semi-complicated central cavities and hypsodonty, features that do not affect the overall shape of the occlusal surface of the tooth (Gentry and Gentry, 1978b, 1978a). The tooth would also be on the small end of the range for a *T. strepsiceros*. Thus, we would consider this tooth an Alcelaphini. We also note that this approach is meant to be a quantifiable supplement to identifying bovids in the fossil record where ambiguity exists, and not the sole method.

The newly identified specimens increase the diversity of fossils recovered from Gladysvale (Table 7). The four alcelaphine species tend to prefer secondary grasslands, short to medium in length (Estes, 2012). Secondary grasses exist where there is minimal woody growth (Reed, 1996). *Oryx gazella* favor open grasslands/savannah with minimal bush cover for hiding. These habitat requirements are consistent with the other species since *D. dorcas*, *A. buselaphus*, and *C. gnou* tend to avoid woodlands while *C. taurinus* requires some shade. The identification of tragelaphines from the site (Lacruz et al., 2002) also confirm that there is some vegetational coverage in the vicinity. The high water dependence of *D. dorcas* and *C. taurinus*, as well as other species previously identified from the site (e.g. *Hippotragus*), suggest a nearby water source (Estes,

Table 5
Shape Features: Species level classifications of the Gladysvale fossil teeth using features generated via elastic shape analysis (I and OV) and classification method SVM-R.

			Hippotragini	Neotragini	Trag	elaphini			
Method	Type	A. buselaphus D.	dorcas C.	gnou C.	taurinus	O. gazella	O. ourebi	T. oryx	T. scriptus
	LM1	1	0	0	0	2	0	1	1
I	LM2	1	0	1	2	0	0	0	0
	LM3	3	0	2	6	0	1	0	0
	UM1	2	0	0	0	1	0	0	0
	UM2	1	0	0	1	0	0	0	0
	UM3	2	1	1	2	0	0	0	0
	Total	10	1	4	11	3	1	1	1
	LM1	1	0	1	0	2	0	0	1
О	LM2	1	0	1	1	1	0	0	0
V	LM3	2	0	1	8	0	1	0	0
	UM1	2	0	0	0	1	0	0	0
	UM2	1	1	0	0	0	0	0	0
	UM3	3	1	1	1	0	0	0	0
	Total	10	2	4	10	4	1	0	1

**Table 6**Size-and-shape Features: Tribe level classifications of the Gladysvale fossil teeth using features generated via elastic shape analysis (I and OV) and classification method SVM-R.

Method	Type	Alcelaphini	Hippotragini	Reduncini	Tragelaphini
I	LM1	5	0	0	0
	LM2	4	0	0	0
	LM3	12	0	0	0
	UM1	2	0	0	1
	UM2	2	0	0	0
	UM3	6	0	0	0
	Total	31	0	0	1
OV	LM1	3	1	0	1
	LM2	4	0	0	0
	LM3	12	0	0	0
	UM1	2	0	1	0
	UM2	1	1	0	0
	UM3	6	0	0	0
	Total	28	2	1	1



**Fig. 12.** Fossil GV8654 reclassified as tragelaphine due to its outline, but the semi-complicated central cavities and hyposodonty of the tooth suggest it is an alcelaphine.

2012). Thus, the bovid identifications support a paleoenvironment that likely consisted of open edaphic and secondary grasslands that grade into bush cover with a local water source. As Lacruz et al. (2002) discussed, it is probable that the excavated fossils represent more than a single environmental event, due to cycles of glacial and interglacial events during the Pleistocene in this region. Further research will be required to identify if multiple habitats may have been sampled.

#### 6. Conclusions

Accurately and objectively identifying the taxonomic classification of fossil Bovidae teeth is of much import in paleoenvironmental reconstruction. Biological anthropologists commonly use the shape of the occlusal surface of specimens to inform their classifications. In the past, when full shapes have been observed elliptical Fourier analysis has been used to derive features for machine learning classification models (Matthews et al., 2018). In this manuscript, a different framework for representing shapes, the square root velocity framework, was explored for its efficacy in deriving features for classification models. Several methods for deriving features as well as several different machine learning models were considered for comparison. We conclude that the feature derivation method referred to here as method I is the best option and the top performing model was a support vector machine with a radial kernel when considering only shape, and this was true for both tribe and species classification. The choice of SVM with a radial kernel as the best choice for a classifier is consistent with the finding of Matthews et al. (2018), which used a different method of feature creation, specifically EFA. We note that while SVM with a radial kernal and method I is best in most cases, there were rare instances where EFA actually did outperform features derived using the elastic shape analysis framework, though in most cases the results were essentially no different or worse.

When size-and-shape features are considered, we observe less variability between the accuracy of different classification methods and methods of feature generation when classifying at the tribe level. With tribe classification, the best performing method was RF with OV-PC used for feature creation, though the improvement over other combinations is smaller than was observed for shape features. Species classification with size-and-shape features based on the random forest slightly outperforms the SVM methods considered here, which is the reverse of what was observed for shape features. Finally, feature generation with EFA was never better than the other methods of feature generation and often quite worse. As a result, one of our main recommendations is that researchers who are using shape or size-and-shape features to perform classification use the elastic shape analysis framework for feature generation.

Table 7
Size-and-shape Features: Species level classifications of the Gladysvale fossil teeth using size-and-shape features generated via elastic shape analysis (I and OV) and classification method SVM-R.

		Alcelaphini			Hippotrag	ini	Reduncini	Tragelaphini	
Method	Туре	A. buselaphus	D. dorcas	C. gnou C. taurinus	O. gazella	H. niger	K. leche	T. strepsicero	s T. oryx
	LM1	1 0	0	2	2	0	0	0 0	
I	LM2	2 0	2	0	0	0	o	0 0	
	LM3	6 0	4	2	0	0	0	0 0	
	UM1	2 0	0	0	0	0	0	1 0	
	UM2	0 0	0	2	0	0	0	0 0	
	UM3	4 1	1	0	0	0	0	0 0	
	Total	15 1	. 7	6	2	0	0	1 0	
	LM1	1 0	0	1	2	0	0	0 1	
OV	LM2	2 0	2	0	0	0	o	0 0	
	LM3	6 1	5	0	0	0	0	0 0	
	UM1	2 0	0	0	0	0	1	0 0	
	UM2	0 0	0	1	0	1	0	0 0	
	UM3	3 1	1	1	0	0	0	0 0	
	Total	14 2	2 8	3	2	1	1	0 1	

Since SVM-R performed well in both shape and size-and-shape settings, we applied this model with feature generation methods I and OV to medium sized alcelaphine fossil specimens from the GVED. When only shape was considered, 18 and 14 out of 32 teeth were classified as Alcelaphini when using feature generation methods I and OV, respectively. When size-and-shape was used, 31 and 28 out of the 32 teeth were classified as Alcelaphini, respectively. The reclassified teeth support and refine the previous paleoenvironmental reconstruction. The reconstructed environment is consistent with other sites in the area dating to a similar time frame. In the future, we plan to apply these methods to more fossils at additional sites.

#### CRediT authorship contribution statement

Juliet K. Brophy: Conceptualization, Data curation, Funding acquisition, Investigation, Writing – original draft, Writing – review & editing. Gregory J. Matthews: Conceptualization, Data curation, Formal analysis, Funding acquisition, Investigation, Methodology, Writing – original draft, Writing – review & editing. Nicole Schnitzler: Formal analysis, Investigation, Methodology, Writing – review & editing. Sebastian Kurtek: Formal analysis, Investigation, Methodology, Writing – review & editing. Ofer Harel: Formal analysis, Investigation, Methodology, Writing – review & editing. Ofer Harel: Formal analysis, Investigation, Methodology, Writing – review & editing.

#### Declaration of competing interest

None

## Acknowledgements

We thank Bernhard Zipfel and Sifelani Jirah, curators at the University of the Witwatersrand, for access to the Gladysvale collections. We also thank LSU Brophy lab student workers Kinsey Van Dyke and Tarun Kakarala.

This work was partially funded by NIH R37-CA214955 (to SK and KB), NSF DMS-2015374 (to GJM and KB), NSF DMS-2015320 (to OH), NSF DMS-2015236 (to JKB), and NSF CCF-1740761, NSF CCF-1839252 and NSF DMS-2015226 (to SK).

#### References

Adams, J., 2012. Revised listing of fossil mammals from the Haasgat cave system ex situ deposits (HGD), South Africa. Palaeontol. Electron. 15 (3), 1–88.

Adams, J., Conroy, G., 2005. Plio-pleistocene faunal remains from the Gondolin GD 2 in situ assemblage, North west Province, South Africa. In: Lieberman, D., Smith, R., Kelley, J. (Eds.), Interpreting the Past: Essays on Human, Primate and Mammal Evolution in Honor of David Pilbeam. Brill Academic Publishers, Boston, pp. 243–261.

Berger, L., Keyser, A., Tobias, P., 1993. Gladysvale: first early hominid site discovered in South Africa since 1948. Am. J. Phys. Anthropol. 92 (1).

Berger, L., Lacruz, R., 2003. Preliminary report on the first excavations at the new fossil site of Motsetse, Gauteng, South Africa. South Africa Journal of Science 99, 279–282. Bharath, K., Kurtek, S., 2020. Analysis of shape data: from landmarks to elastic curves. WIREs Computational Statistics 12, e1495.

Bonhomme, V., Picq, S., Gaucherel, C., Claude, J., 2014. Momocs: outline analysis using R. J. Stat. Software 56 (13), 1–24.

Breiman, L., 2001. Random forests. Mach. Learn. 45, 5–32.

Brink, J., 1987. The archaeozoology of Florisbad, Orange free state. Mem. Nas. Mus. Bloemfontein 24.

Brink, J., 2005. The Evolution of the Black Wildebeest, Connochaetes Gnou, and Modern Large Mammal Faunas in Central Southern Africa. PhD thesis. University of Stellenbosch.

Brink, J., Herries, A., Moggi-Cecchi, J., Gowlett, J., Bousman, C., Hancox, J., Grün, R., Eisenmann, V., Adams, J., Rossouw, L., 2012. First hominine remains from a 1.0 million year old bone bed at Cornelia-Uitzoek. J. Hum. Evol. 63 (3), 527–535.

- Brophy, J., 2011. Reconstructing the Habitat Mosaic Associated with Australopithecus Robustus: Evidence from Quantitative Morphological Analysis of Bovid Teeth. PhD thesis. Texas A&M University, College Station, Texas, USA.
- Brophy, J., de Ruiter, D., Athreya, S., DeWitt, T., 2014. Quantitative morphological analysis of bovid teeth and its implications for paleoenvironmental reconstruction of Plovers Lake, Gauteng Province, South Africa. J. Archaeol. Sci. 41, 376–388.
- Brophy, J., Matthews, G., 2022. Reference database of teeth images from the Family Bovidae. Sci. Data 9 (1), 396.
- Caple, J., Byrd, J., Stephan, C., 2017. Elliptical Fourier analysis: fundamentals, applications, and value for forensic anthropology. Int. J. Leg. Med. 131, 1675–1690. Cortes, C., Vapnik, V., 1995. Support-vector networks. Mach. Learn. 20 (3), 273–297.
- de Ruiter, D., Brophy, J., Lewis, P., Churchill, S., Berger, L., 2008. Faunal assemblage composition and paleoenvironment of Plovers Lake, a middle stone age locality in Gauteng Province, South Africa. J. Hum. Evol. 55 (5), 1102–1117.
- Domínguez-Rodrigo, M., Brophy, J., Matthews, G., Pizarro-Monzo, M., Baquedano, E., 2023. African bovid tribe classification using transfer learning and computer vision. Ann. N. Y. Acad. Sci. 1530 (1), 152–160.
- Estes, R., 2012. The Behavior Guide to African Mammals: Including Hoofed Mammals, Carnivores, Primates. Univ of California Press.
- Gentry, A., Gentry, A., 1978a. Fossil Bovidae (Mammalia) of Olduvai gorge, Tanzania part 2. Bulletin of the British Museum (Natural History) Geology Series 30 (1), 1–83.
- Gentry, A.W., Gentry, A., 1978b. Fossil Bovidae (mammalia) of olduvai gorge, Tanzania part 1. Bulletin of the British Museum (Natural History) Geology Series 29 (4), 289 446
- Hall, G., Pickering, R., Lacruz, R., Hancox, J., Berger, L., Schmid, P., 2006. An acheulean handaxe from Gladysvale cave site, Gauteng, South Africa: research in action. South Afr. J. Sci. 102 (3), 103–105.
- Ho, T., 1995. Random decision forests. In: Proceedings of 3rd International Conference on Document Analysis and Recognition., vol. 1. IEEE, pp. 278–282.
- James, G., Witten, D., Hastie, T., Tibshirani, R., 2023. An Introduction to Statistical Learning with Applications in R, second ed. Springer.
- Kurtek, S., Srivastava, A., Klassen, E., Ding, Z., 2012. Statistical modeling of curves using shapes and related features. J. Am. Stat. Assoc. 107 (499), 1152–1165.
- Lacruz, R.S., Brink, J., Hancox, P., Skinner, A.R., Herries, A., Schmid, P., Berger, L.R., 2002. Palaeontology and geological context of a middle Pleistocene faunal assemblage from the Gladysvale cave, South Africa. Palaeontol. Afr. 38 (99), e114.

- Liaw, A., Wiener, M., 2002. Classification and regression by randomForest. R. News 2 (3), 18–22.
- Matthews, G., Brophy, J., Luetkemeier, M., Gu, H., Thiruvathukal, G., 2018.

  A comparison of machine learning techniques for taxonomic classification of teeth from the Family Bovidae. J. Appl. Stat. 45 (15), 2773–2787.
- Meyer, D., Dimitriadou, E., Hornik, K., Weingessel, A., Leisch, F., 2023. e1071: Misc Functions of the Department of Statistics, Probability Theory Group (Formerly: E1071), TU Wien. R package version 1, 7–13.
- Mio, W., Srivastava, A., Joshi, S., 2007. On shape of plane elastic curves. Int. J. Comput. Vis. 73 (3), 307–324.
- Pickering, R., Hancox, P., Lee-Thorp, J., Grün, R., Mortimer, G., McCulloch, M., Berger, L., 2007. Stratigraphy, U-Th chronology, and paleoenvironments at Gladysvale Cave: insights into the climatic control of South African hominin-bearing cave deposits. J. Hum. Evol. 53 (5), 602–619.
- Powers, S., Hastie, T., Tibshirani, R., 2018. Nuclear penalized multinomial regression with an application to predicting at bat outcomes in baseball. Stat. Model. Int. J. 18, 388–410.
- R Core Team, 2021. R: A Language and Environment for Statistical Computing. R Foundation for Statistical Computing.
- Reed, K., 1996. The Paleoecology of Makapansgat and Other African Plio-Pleistocene Hominid Localities. PhD thesis. State University of New York, Stony Brook.
- Robinson, D., 2012. Functional Data Analysis and Partial Shape Matching in the Square Root Velocity Framework. Florida State University. PhD thesis.
- Srivastava, A., Klassen, E., 2016. Functional and Shape Data Analysis. Springer, New York, NY.
- Srivastava, A., Klassen, E., Joshi, S., Jermyn, I., 2011. Shape analysis of elastic curves in Euclidean spaces. IEEE Trans. Pattern Anal. Mach. Intell. 33, 1415–1428.
- The GIMP Development Team, 2019. GNU Image Manipulation Program (GIMP).
- Vrba, E., 1976. The fossil Bovidae of sterkfontein, swartkrans and kromdraai. Transvaal Museum Memoir 21 (21).
- Vrba, E., 1997. New fossils of Alcelaphini and caprinae (Bovidae: Mammalia) from Awash, Ethiopia, and phylogenetic analysis of Alcelaphini. Palaeontol. Afr. 34, 127–198.